Article

Non-temperature environmental drivers modulate warming-induced 21st-century permafrost degradation on the Tibetan Plateau

Ziteng Fu[1,2,5], Qingbai Wu ®[1,2,3,5] ✉, Anping Chen[4], Luyang Wang[1], Guanli Jiang ®[1,3], Siru Gao[1], Hanbo Yun ®[1,3] & ji Chen[1,3]

The world's largest continuous alpine permafrost layer on the Tibet Plateau (TP), is increasingly threatened by warming leading permafrost degradation that disrupts carbon, water, and nutrient cycling, and threatens ecosystem services and infrastructure stability. However, it remains unclear how permafrost sensitivity to warming varies across the TP and over time. By compiling a 20-year (2001–2020) dataset from 55 in situ monitoring sites, we find permafrost thawing rates increased from 45 ± 15 cm·10a^{-1} (2001–2010) to 86 ± 30 cm·10a^{-1} (2011-2020), while the temperature increasing rates at the top of permafrost rose from 0.15 ± 0.16 °C·10a^{-1} to 0.38 ± 0.22 °C·10a^{-1}. Temperature explains 18% and 17% of the observed changes in active layer thickness and permafrost temperature, respectively, while non-temperature variables collectively account for 45%. Notably, precipitation patterns exert contrasting effects on permafrost: Increasing precipitation south of 34°N leads to active layer thinning and permafrost cooling, while in the north it deepens the active layer and warms permafrost. Our findings underscore the crucial role of non-temperature variables in modulating permafrost responses to climate change, which is important for refining projections of carbon, nutrient, and water cycling and for safeguarding critical infrastructures in the TP and other permafrost regions.

Permafrost, or permanently frozen soil layers, covers approximately 17% of Earth' land surface[1] and store about 50% of its soil carbon within the top three meters[2]. These regions are experiencing some of the most rapid temperature increases worldwide, threatening ecosystems and communities that depend on permafrost stability[3,4]. In particular, warming accelerates permafrost thaw—commonly referred to as "permafrost degradation"—with profound implications for carbon, nutrient, and water cycles, as well as for man-made infrastructure[5–7]. As thawing releases organic matter previously locked in frozen soils, large quantities of carbon dioxide and methane are emitted into the atmosphere, amplifying climate change[2,8]. Infrastructure, including roads, pipelines, and buildings, is also at risk as once-solid ground begins to settle and destabilize[9,10]. Given these wide-ranging impacts, there is an urgent need to improve our understanding of permafrost's

[1]State Key Laboratory of Cryospheric Science and Frozen Soil Engineering, Northwest Institute of Eco-Environment and Resources, Chinese Academy of Science, Lanzhou 730000, China. [2]University of Chinese Academy of Sciences, Beijing 100049, China. [3]Qinghai-Beilu Plateau Frozen Soil Engineering Safety National Observation and Research Station, Chinese Academy of Sciences, Lanzhou 730000, China. [4]Department of Biology and Graduate Degree Program in Ecology, Colorado State University, Fort Collins, CO, USA. [5]These authors contributed equally: Ziteng Fu, Qingbai Wu. ✉e-mail: qbwu@lzb.ac.cn

vulnerability to climate change[11–13] to better predict future changes, manage risks, and develop adaptation strategies[1,4,14].

The Tibetan Plateau (TP) hosts the world's largest continuous alpine permafrost area[15] and has experienced particularly rapid warming—roughly twice the global average[16]. This region's permafrost is highly sensitive to air temperature increases[17], with strong impacts on both ecosystems[18] and human society[19,20]. Importantly, as the "Roof of the World", changes in permafrost processes on the TP can disrupt regional land-atmosphere interactions[21] and hydrological cycling[22], influencing summer rainfall in downstream areas such as the Yangtze River Basin and southern Japan[21]. These broad-scale effects underscore the importance of quantifying spatial and temporal variations in permafrost degradation across the TP and understanding how these variations are influenced by multiple environmental factors.

Empirical evidence of permafrost degradation across the TP has been widely reported[16,23,24]. On average, the permafrost warming rate on the TP is 0.17 ± 0.11 °C per decade from 1996 to 2014[25], which is slower than the rates observed in the Arctic[4], the European mountains[26], and the global average[3]. This is because the rapid thawing of warm permafrost, accompanied by heat absorption from the partial melting of interstitial ice, slows and attenuates permafrost temperature increasing[27]. Meanwhile, the active layer thickness (ALT) in the TP has increased at a rate of 46.7 ± 26.9 cm per decade[25]. However, these average rates do not capture the whole picture, as the TP's diverse climatic, vegetation, and topographical conditions create high spatial heterogeneities in permafrost changes[23,28]. Nonetheless, due to the harsh environment and logistical challenges of the TP, most previous studies have relied on limited sites and short-term monitoring data[16,23,24], leaving key gaps in our understanding of spatiotemporal variability and drivers of permafrost change. Filling this gap is critical for predicting how permafrost will respond to the TP's accelerating warming[29,30].

Moreover, although rising air temperatures are strongly correlated with permafrost degradation[3,4,31,32], temperature alone explain only a limited portion of the observed inter-annual variability and long-term trends[4,33]. Other environmental factors, such as precipitation, snow cover, vegetation, and topography, also play important roles in modulating permafrost dynamics[4,34,35]. Empirical evidence quantifying these non-temperature influences, however, remains sparse[28], constraining our understanding of permafrost sensitivity and its implications for ecological and engineering stability and for carbon and nutrient cycle assessments.

Here, we address these knowledge gaps by compiling a unique 20-year (2001–2020) dataset of in situ permafrost monitoring from 55 sites across the TP (Supplementary Fig. 1 and Supplementary Table 1), encompassing diverse climatic, vegetation, edaphic, and topographic conditions. This dataset may serve as a previously unavailable baseline for evaluating permafrost changes in the TP. We systematically assess the spatiotemporal variability of permafrost change and the relative influence of four categories of environmental drivers: (1) temperature, (2) non-temperature climate variables (e.g., precipitation, wind speed, radiation), (3) edaphic and vegetation factors (e.g., soil characteristics, plant cover), and (4) geophysical factors (e.g., altitude, latitude). Our findings offer critical insights into the mechanisms of permafrost change, with important implications for understanding regional carbon, water, and nutrient cycles under climate change and for maintaining infrastructure stability in this sensitive and rapidly changing landscape.

Results
Spatial and temporal variations in permafrost changes
We first investigate spatial and temporal variations in key permafrost variables, including active layer thickness (ALT), temperature at the top of permafrost (TTOP), and permafrost temperature at depths of 10 m (PT_{10m}) and 15 m (PT_{15m}), utilizing continuously recorded data on soil temperature within the active layer and permafrost from 2001–2020. We apply Mann-Kendall trend tests and linear regression through least squares (see methods) to determine trends in ALT and permafrost temperatures (i.e., TTOP, PT_{10m}, and PT_{15m}), as well as their rates of change across 5-year running windows. The results show that from 2001–2020, ALT increased significantly, deepening from 2.79 ± 0.92 m in the first decade (2001-2010) to 3.52 ± 1.15 m in the last decade (2011–2020; Supplementary Fig. 2), at an average rate of 63 ± 3.6 cm·10a^{-1} ($p < 0.01$). Furthermore, the change rate in ALT also increased from 45 ± 15 cm·10a^{-1} in the first decade to 86 ± 30 cm·10a^{-1} in the last decade (Supplementary Fig. 2). This increasing rate of 41 ± 13 cm·10a^{-2} is also significant with 5-year running windows from 2001 to 2020 ($p < 0.05$; Fig. 1c).

Using unbalanced group box plots, we find that different geomorphic units—including mountain areas, basins, high-plains, and valleys—show significantly distinct characteristics and change rates in ALT (Fig. 1b). Generally, mountain areas show a lower mean ALT (1.85 ± 0.46 m) and a slower mean change rate (4.4 ± 2.5 cm·10a^{-1}) compared to basins, high plains, and valleys (Fig. 1b). Valleys have the highest mean ALT (4.18 ± 1.32 m), although their ALT change rate (9 ± 8 cm·10a^{-1}) is smaller than that of the basins (49 ± 17 cm·10a^{-1}) and high plains (65 ± 54 cm·10a^{-1}). Vegetation cover also significantly influences ALT. The mean ALT is lowest in alpine meadows compared to alpine steppes and alpine desert steppes, with the rate of change also being slightly slower in alpine meadows than in the other vegetation types (Fig. 1b). Furthermore, ALT decreases with increasing altitude at the same latitude (Supplementary Fig. 3) and deepens with decreasing latitude at the same altitude (Supplementary Fig. 4). Latitude notably controls the spatiotemporal changes in ALT along the altitude gradient (Fig. 1d). The local impact of vegetation cover and topography results in a stronger latitudinal zonality compared to altitudinal effects.

Along with the increasing ALT from 2001 to 2020, TTOP rose from an average of -0.88 ± 0.72°C in the first decade to -0.61 ± 0.65 °C in the last decade (Supplementary Fig. 5), with a significant upward trend at an average rate of 0.27 ± 0.03 °C·10a^{-1} ($p < 0.01$). Similar to ALT changes, the change rate in TTOP also increased from 0.15 ± 0.16 °C·10a^{-1} in the first decade to 0.38 ± 0.22 °C·10a^{-1} in the last decade (Supplementary Fig. 5). The 5-year running window analysis showed an increasing rate of 0.025 ± 0.01 °C·10a^{-2} from 2001 to 2020 (Fig. 2a). Additionally, PT_{10m} and PT_{15m} also exhibited warming trends, with average rates of 0.18 ± 0.06 °C·10a^{-1} and 0.14 ± 0.04 °C·10a^{-1} ($p < 0.01$), respectively (Fig. 2a). Although the rising trends of PT_{10m} and PT_{15m} were significant, the increasing rate by 5-year running windows was not significant (Fig. 2a). The changes in PT_{10m} and PT_{15m} between the first and last decade were roughly equivalent (Supplementary Fig. 5). Overall, these results indicate that near-subsurface permafrost is experiencing a significantly accelerated rate of thawing and warming (Supplementary Table 2).

Significant differences in permafrost temperature characteristics and their changes are also found across different geomorphic units and vegetation types (Fig. 2). In general, mean permafrost temperatures are lowest in maintain areas, yet these regions also experience the highest rates of temperature increase compared to basins, high plains, and valleys (Fig. 2b). Regarding vegetation types, alpine meadow has the lowest TTOP, PT_{10m} and PT_{15m}, but the highest rates of change (Fig. 2c). This pattern suggests that areas with the lowest permafrost temperature often face the most rapid warming. Additionally, both the temperature characteristics and changes in the TP permafrost region exhibit pronounced zonality along altitude and latitude gradients (Supplementary Fig. 3 and 4). For example, temperature increases with decreasing latitude when controlling for altitude, and vice versa (Supplementary Fig. 4). Using Pearson correlation analysis (see Methods), we find notable changes in the relationship between Pre and both ALT and permafrost temperature variables at around the
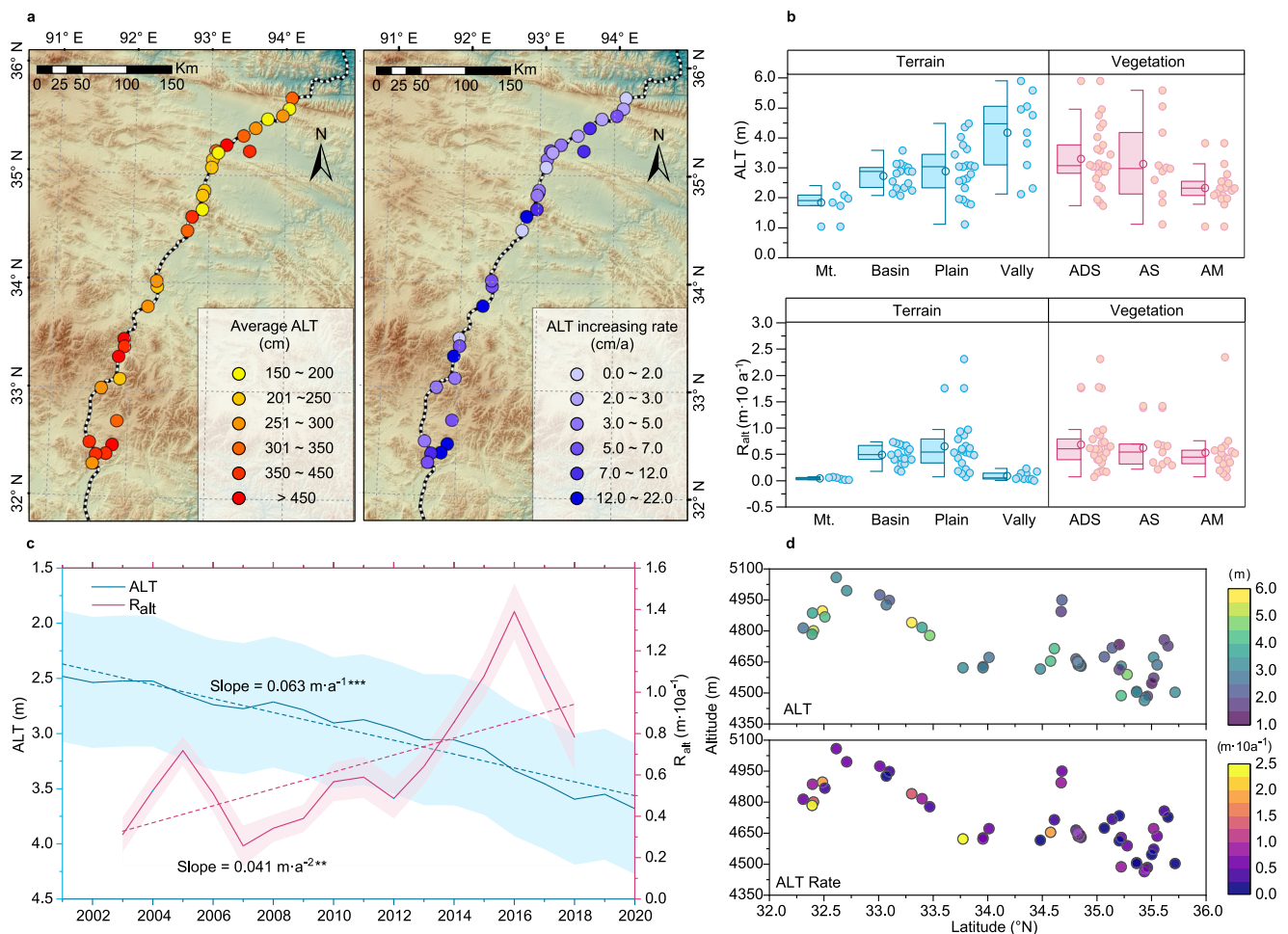
Fig. 1 | Change in active layer thickness (ALT) on the Tibetan Plateau. a Mean values and change rates (R_{alt}) of ALT, represented by the color intensity of the bubbles. b Unbalanced group box plots of ALT and R_{alt} for different terrain types–mountain areas (Mt.), basin (Basin), high plains (Plain), and valleys (Valley)–as well as for vegetation types: alpine desert steppe (ASD), alpine steppe (AS), and alpine meadow (AM). Each group includes a box plot on the left and a corresponding scatterplot on the right. In the box plots, the box spans the interquartile range (IQR, 25th to 75th percentiles), the horizontal line represents the median, and whiskers extend to 1.5 times the IQR beyond the quartiles. Topographic base maps used in a and b were generated by the authors using the ALOS PALSAR digital elevation model (20 m resolution), © JAXA/METI, accessed via the NASA Alaska Satellite Facility (ASF). c Trends and rates over a 5-year running window from 2001 to 2020. Bold lines indicate observed values (means of all sites) and dashed lines are trends estimated by linear regression. Rates were estimated using a 5-year moving window approach, with the value plotted for a given year representing the trend calculated over the 5-year window centered on that year (e.g., 2003 represents the trend for 2001-2005). Shaded areas indicate 95% confidence intervals for ALT and its change rates. Asterisks denote statistical significance (***$p < 0.001$; **$p < 0.01$; *$p < 0.05$). d Spatial distribution of ALT and its change rate, with bubble color intensity indicating magnitude.

34°N latitude (Fig. 4). Increases in precipitation lead to thinning of the ALT and cooling of the permafrost south of 34°N, whereas resulting in deeper ALT and warmer permafrost north of this line (Fig. 3). For each latitude band, the strengths of such relationships are also influenced by altitude. Latitude also significantly influences the spatiotemporal dynamics of permafrost temperature changes along the altitude gradient (Fig. 2d).

Attributing variations in permafrost changes to different factors
To investigate the role of different environmental factors in shaping the spatiotemporal variation in ALT and permafrost temperature on the TP, we focus the analysis on seven climate variables and various non-climate environmental factors. The climate variables include air temperature (T_a) and six non-temperature variables: precipitation (Pre), solar radiation (Sr), wind speed (Ws), specific humidity (St), surface pressure (Sp), and freezing level height (FLH). Non-climate environmental factors include: (1) topography factors (slope and roughness), (2) vegetation factors (vegetation cover), (3) geographic

factors (altitude and latitude), and (4) permafrost state variables (ALT, TTOP, PT_{10m}, PT_{15m} and ice content near the top of permafrost). We analyze the contributions of these variables to the observed spatio-temporal changes in ALT and permafrost temperatures through the variance decomposition analysis (see methods). Specifically, the selection of relevant climate variables and non-climate environmental factors is first conducted via cluster analysis (see methods; Supplementary Fig. 6). Explanatory variables form a matrix that includes ALT (and its variability), permafrost temperatures (and their variabilities), as well as the correlations among these variables (Supplementary Fig. 7).

Using the Lindeman-Merenda-Gold (LMG) method and a correlation coefficient matrix (see methods), we find that air temperature can explain about 18% and 22% of the variations in ALT and TTOP, respectively (Fig. 4a). As a comparison, non-temperature climate factors collectively account around 45% for ALT and TTOP, much larger than that explained by air temperature (Fig. 4a). This result suggests that, while air temperature is an important driver of permafrost
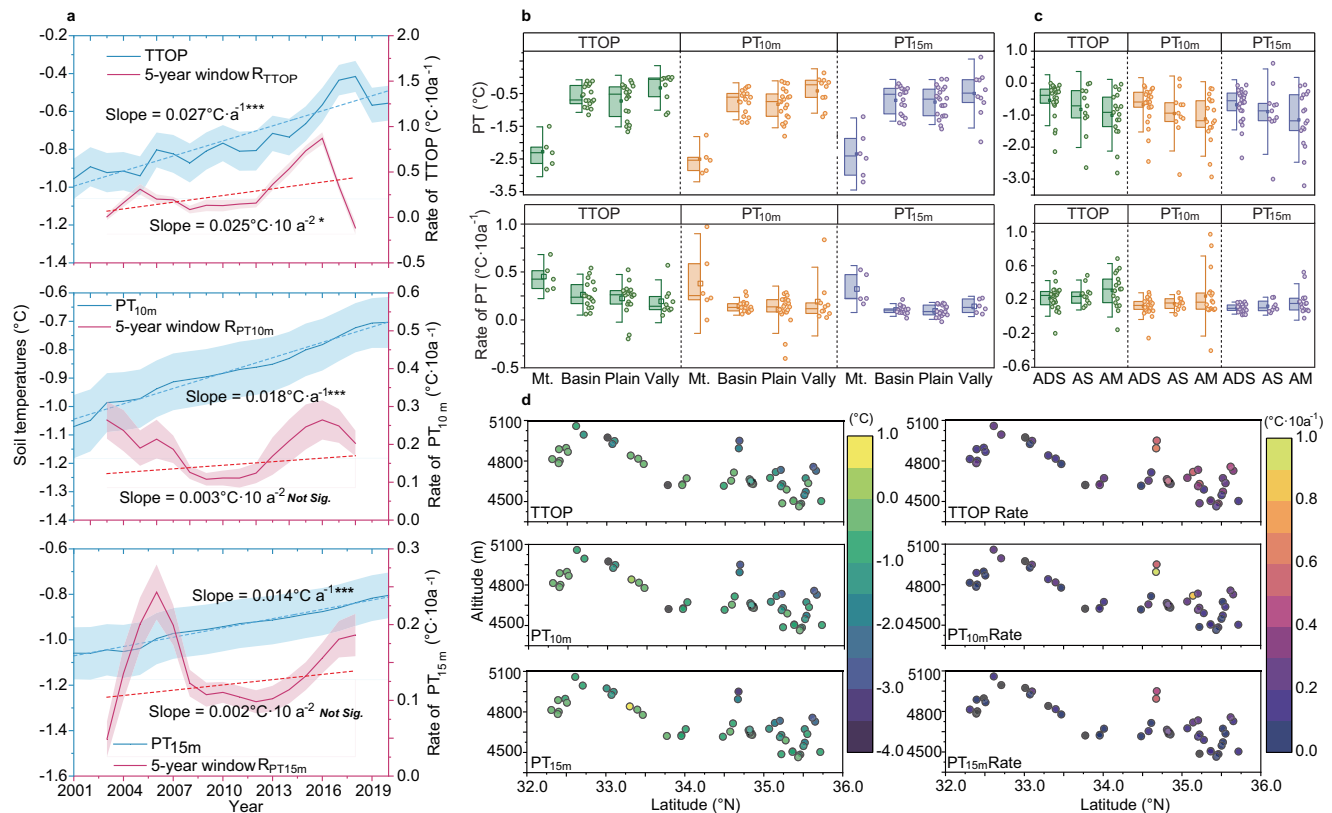
Fig. 2 | Changes in permafrost temperature on the Tibetan Plateau. a Trends and rates of temperature changes at the top of permafrost (TTOP), and at depths of 10 m (PT_{10m}) and 15 m (PT_{15m}), based on a 5-year running window from 2001 to 2020. Bold lines are observations (means of all sites), and dashed lines are trends estimated by linear regression. Rates were estimated using a 5-year moving window, with the value plotted for a given year representing the trend calculated over the 5-year window centered on that year (e.g., 2003 represents the trend for 2001-2005). Shaded areas indicate 95% confidence intervals for permafrost temperatures and their change rates. Asterisks denote statistical significance (***$p < 0.001$; **$p < 0.01$; *$p < 0.05$). **b** Unbalanced group box plots of TTOP, PT_{10m}, and PT_{15m} and their change rates for different terrain types: mountain areas (Mt.), basin (Basin), high plain (Plain), and valleys (Valley). **c** Unbalanced group box plots of different vegetation types: alpine desert steppe (ASD), alpine steppe (AS) and alpine meadow (AM). Each group includes a box plot on the left and a corresponding scatterplot on the right. In the box plots, the box spans the interquartile range (IQR, 25th to 75th percentiles), the horizontal line represents the median, and whiskers extend to 1.5 times the IQR beyond the quartiles. **d** Spatial distributions of TTOP, PT_{10m}, and PT_{15m} and their change rates, with bubble color intensity indicating magnitude.

changes, other environmental variables (e.g., precipitation and soil properties) may play an even more influential role at regional scales. Among the non-temperature climate variables, FLH emerges as the most important, accounting for approximately 13% of the changes in ALT and TTOP. Wind speed and surface pressure are also critical, collectively explaining roughly 20% of variations in ALT and TTOP changes. Precipitation and solar radiation together account for 12% and 9% of variations in ALT and TTOP changes, respectively (Fig. 3a). Notably, excluding FLH and surface pressure from the analysis can lead to a substantial overestimation of the influence of air temperature, with overestimations exceeding 50% (Supplementary Fig. 8).

Furthermore, the influence of climate variables on deeper permafrost warming shows a marked contrast compared to TTOP changes (Fig. 4a). While air temperature remains the most critical variable affecting deeper permafrost warming, it accounts for less than 15% of the explanatory power (Fig. 3b). The collective impact of non-temperature climate variables on permafrost warming is much larger, explaining about 45% of the variations (Fig. 4a).

There are also substantial differences in the contributions of various factors to the spatiotemporal variation in permafrost state variables and their change rates (Fig. 4b). For example, air temperature accounts for less than 10% of the variation in spatial changes in permafrost characteristics, significantly smaller than the 39.1% attributed to non-temperature factors, which include vegetation types, geographic and topographic elements, and soil water content near the top of permafrost. Additionally, air temperature explains only 3% of the

spatial variation in permafrost change rates, with non-temperature factors accounting for 13.6%.

When combined, all these climate variables and environmental factors together explain only a minimal portion of the spatial variation in permafrost change rates, accounting for 16.6%. However, permafrost state variables can explain 12.1% the spatial variation in permafrost change rates (Fig. 4b). In addition, about 27% of the variations in permafrost state variables and 45.8% of the variations in their change rates cannot be explained by our selected variables. This underscores the complexity of permafrost dynamics on the Tibetan Plateau, which is shaped and controlled by a myriad of regional and local factors.

Impacting pathway of climate variables and environmental factors on permafrost degradation

We also employ structural equation modeling (SEM) to further disentangle the complex roles of climate and non-climate variables in driving permafrost changes. The results show good fits, with $\chi^2/df = 1.594$, $p < 0.001$, GFI = 0.997, AGFI = 0.797, and RMSE = 0.027 (Fig. 5). The SEM paths reveal that vegetation cover, soil temperature within the active layer, FLH, and climatic factors represented by the first component of principal component analysis (PC1) scores directly influence permafrost characteristics, explaining 64.9% of their spatial variations (Fig. 5). Specifically, soil temperature within the active layer has a substantial positive effect (43.2%), while vegetation cover exhibits a significant negative effect (38.8%). Furthermore, topography, climate variables, vegetation cover, soil water content, and permafrost
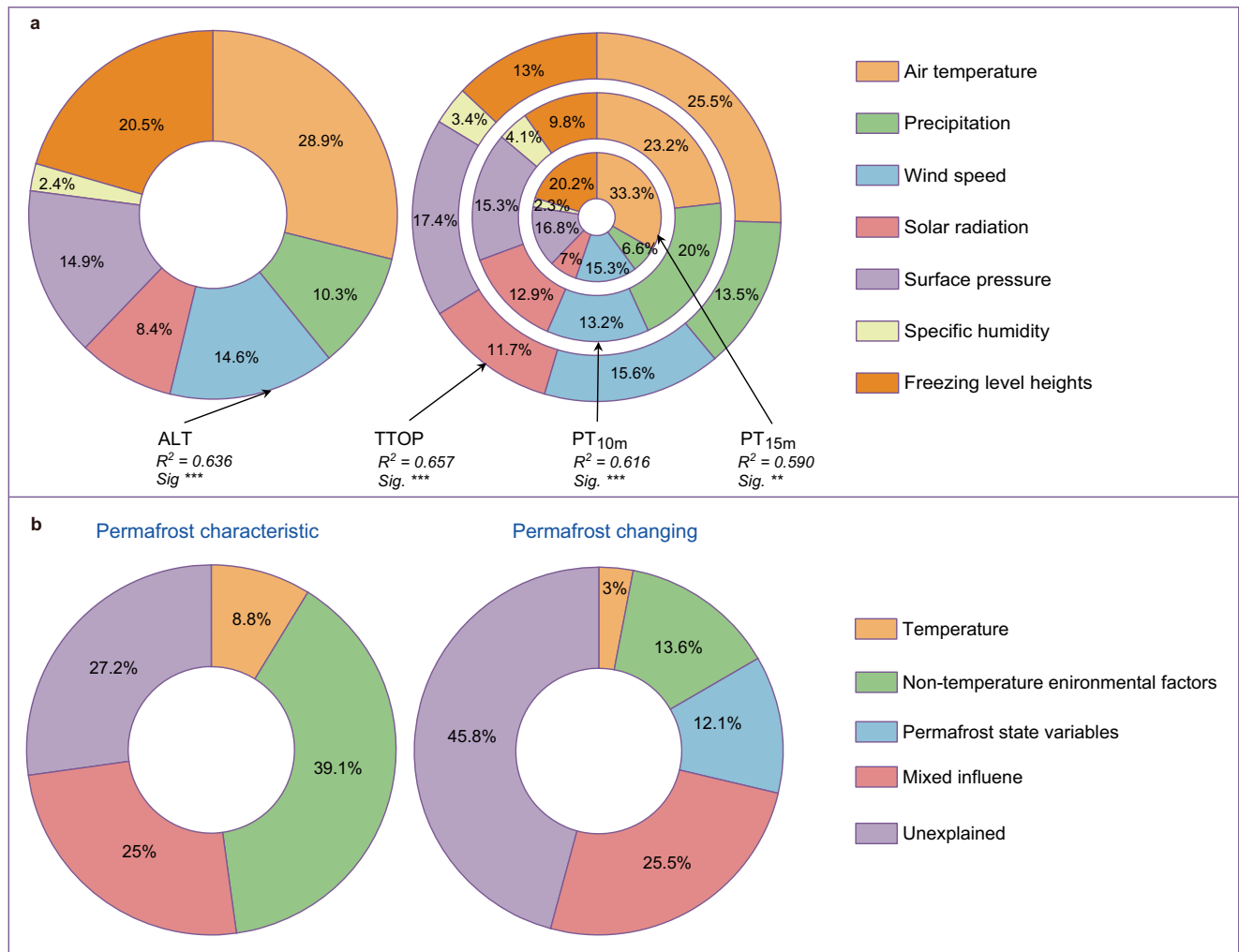
Fig. 3 | Relative contributions of climate and environmental factors to permafrost characteristics and changes. a Relative importance of climate variables in explaining the temporal variation of active layer thickness (ALT) and permafrost temperatures. **b** Contributions of environmental factors to spatial variation in permafrost characteristics and changes. Relative importance was assessed using the Lindeman–Merenda–Gold (LMG) method (see Methods), based on climate data from 2001 to 2018, including air temperature, precipitation, wind speed, solar radiation, surface pressure, specific humidity, and freezing level height. Prior to the LMG analysis, correlation coefficients and significance levels between climate variables and permafrost characteristics were calculated using multiple region analysis to examine the impact of climate change on permafrost characteristics ($p < 0.05$). Variation partitioning analysis (VPA) was applied to partition variances of permafrost characteristics—active layer thickness (ALT), temperature at the top of permafrost (TTOP), and permafrost temperatures at 10 m (PT_{10m}) and 15 m (PT_{15m}) depths—and their change rates among temperature factors (air temperature and land surface temperature), non-temperature factors, and permafrost state variables.

characteristics influence permafrost changes, collectively accounting for 36.9% of these changes. A significant interaction is identified among climate variables, non-climate environmental factors, and permafrost state variables and their changes, highlighting that the interaction between the land surface and the atmosphere acts as a pivotal factor impacting permafrost characteristics and their temporal changes, with notable zonality differences. FLH, explaining 25.8% of permafrost characteristics and 10.5% of permafrost changes, likely plays a critical role in this interaction, suggesting that atmospheric circulation near the surface can directly alter the spatiotemporal dynamics of permafrost. Moreover, the direct effect of permafrost characteristics on permafrost changes is up to 59%, with a strong inverse correlation between the spatial characteristics of permafrost and its temporal changes (Fig. 5a). This indicates that the variability of permafrost change is largely dependent on the inherent state of the permafrost thermal regime and ALT, influenced by different topographies and vegetation covers (Fig. 5a).

Discussion

Our study reveals the accelerated degradation of permafrost in the TP, highlighting the influence of non-temperature climate variables and environment factors. Specifically, the thawing rate of permafrost, as well as the temperature increasing rate at the top of permafrost, has nearly doubled over the past two decades (Supplementary Figs. 2 and 5), providing a more complete quantification of permafrost degradation that has not been documented before. As a comparison, the warming trends of the deeper permafrost (10m depth and 15m depth) have not changed significantly between 2010s to 2000s, suggesting the dominant role of sub-surface warming in TP's permafrost degradation. Our findings challenge the current understanding of permafrost sensitivity to climate change and highlight the importance of incorporating non-temperature variables into models projecting future permafrost dynamics.

It is important to note that the permafrost monitoring data in this study were point-scale measurements, while the climate data were
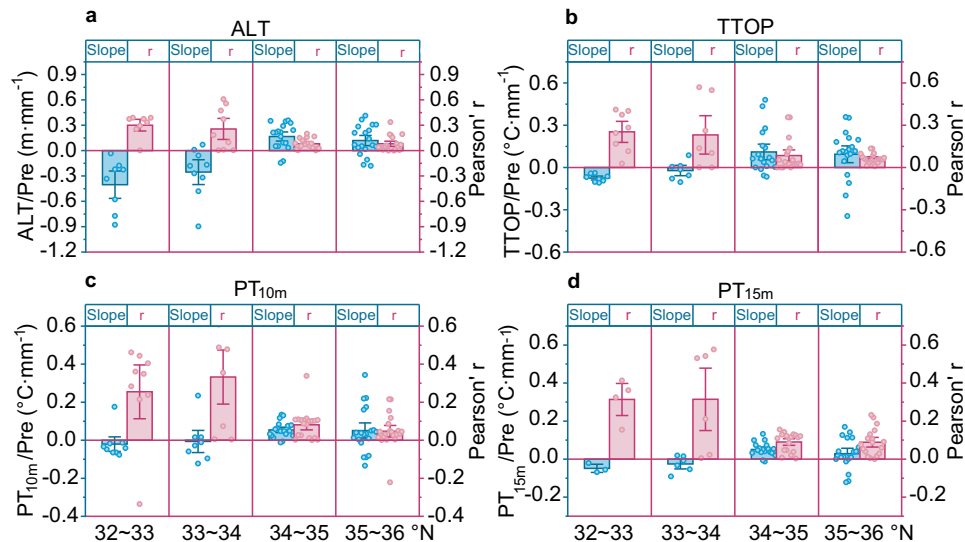
Fig. 4 | Latitudinal zonation of permafrost sensitivity to changes in precipitation. Sensitivity of four key attributes is shown: **a** active layer thickness (ALT), **b** temperature at the top of permafrost (TTOP), **c** permafrost temperature at a depth of 10 m (PT_{10m}), and **d** permafrost temperature at a depth of 15 m (PT_{15m}). Sensitivity is defined as the slope of each permafrost attribute (ALT, TTOP, PT_{10m}, PT_{15m}) with respect to changes in precipitation, determined through linear regression analysis. Error bars in **a**–**d** represent the standard errors of the slope and Pearson's correlation coefficient (r).

derived from gridded datasets (e.g., TPDC, TRMM). Although these gridded datasets provide valuable long-term, regional-scale coverage, their spatial resolution may not adequately capture local variability at each monitoring site. This scale mismatch introduces uncertainties into our attribution analysis, especially regarding the effects of air temperature and precipitation on ALT and TTOP. Although the gridded data showed strong consistency with station observations in terms of both long-term trends and inter-annual variability (Supplementary Fig. 15), the estimated contributions of air temperature and precipitation to permafrost dynamics should be interpreted with caution. In particular, the relatively lower contribution of air temperature (18% and 22% for ALT and TTOP, respectively) may partly reflect the smoothing effect inherent in gridded datasets, which can underestimate site-level temperature variability. Future studies using high-resolution downscaled climate data or station-based interpolations may improve the precision of climate-permafrost attribution analysis.

Multiple climate and environment factors have been demonstrated crucial in driving permafrost degradation in the TP[16,23,30,36]. Since the 1980s, the TP has experienced significant changes in climate: air temperature has increased by $0.36 \pm 0.08\,°C$ per decade, precipitation by 51.2 ± 0.08 mm per decade, solar radiation by $1.16 \pm 0.52\,W/m^2$ per decade, and wind speed by 0.39 ± 0.07 m/s per decade (Supplementary Fig. 9). However, over the past 20 years, although air temperature has continued to show a significant increasing trend, changes in precipitation, wind speed, solar radiation, surface pressure, and specific humidity have been relatively insignificant (Supplementary Fig. 10). This rising temperature is a key factor driving permafrost degradation over the past two decades. However, non-temperature climate variables, such as FLH and surface pressure, could lead to a structural change in how warming impacts permafrost changes (Supplementary Fig. 8). It appears that the impact of temperature on permafrost change may be overestimated without considering FLH and surface pressure. These variables enhance the significance and R² values of the relationships among climate variables and permafrost changes (Supplementary Figs. 8 and 4a). Therefore, FLH and surface pressure emerge as important factors influencing changes in ALT and permafrost temperature. These important findings have not been previously considered and warrant further investigation to understand their mechanisms in regulating permafrost changes (Supplementary Fig. 11). Including the influence of these factors in

simulations of permafrost distribution and ground temperature could greatly reduce the uncertainty in models.

Snow cover on the TP is predominantly found in high mountainous areas, with relatively shallow snow depths in the plateau's relatively flat inlands[36]. Over the past 50 years, approximately 70% of meteorological stations in the region have recorded an average of fewer than 30 snow cover days per year, and about 77% of stations have reported an average daily snow depth of less than 0.5 cm[37]. Given these low values of snow cover depth and duration, their impact on permafrost is considered limited, which might have already been included in the impact of annual precipitation. Hence, here we do not include snow cover in the climate variables or underlying surface factors.

Rainfall influences soil thermal conductivity, heat capacity, heat flux, and evapotranspiration through altering soil water availability, which can either a cooling or warming effect on permafrost degradation[38–40]. However, research on the impact of precipitation on permafrost dynamics is rather limited[40]. The scarcity of precipitation observations in the TP's permafrost regions, coupled with considerable measurement errors[41], contribute to the uncertainty regarding precipitation's role in permafrost degradation. Interestingly, results of our in situ monitoring show a clear reversal in the impact of precipitation on permafrost degradation north and south of 34°N (Fig. 4). From 2001 to 2020, precipitation trends indicate a wetting pattern north of 34°N and drying south of 34°N (Supplementary Fig. 12). In the drier northern area, increased rainfall mitigates permafrost degradation by enhancing soil heat capacity and reducing soil heat through evapotranspiration[39]. However, further precipitation increases would improve soil thermal conductivity and latent heat transfer, accelerating permafrost thawing[38] (Supplementary Fig. 13). In the wetter southern region, increased rainfall promotes permafrost degradation by boosting soil heat through enhancing thermal conductivity and infiltration, while reduced precipitation slightly decreases vertical heat flux due to minimal changes in thermal conductivity during soil drying[38]. Despite decreased rainfall, high latent heat transfer continues, leading to accelerating permafrost thawing (Supplementary Fig. 13). Thus, while precipitation changes north and south of 34°N contribute to permafrost degradation, the rate is influenced by factors such as soil water content, organic material content, vegetation, and ground ice[38]. This finding highlights the potential for increased uncertainty in permafrost changes under future warming-wetting scenarios.

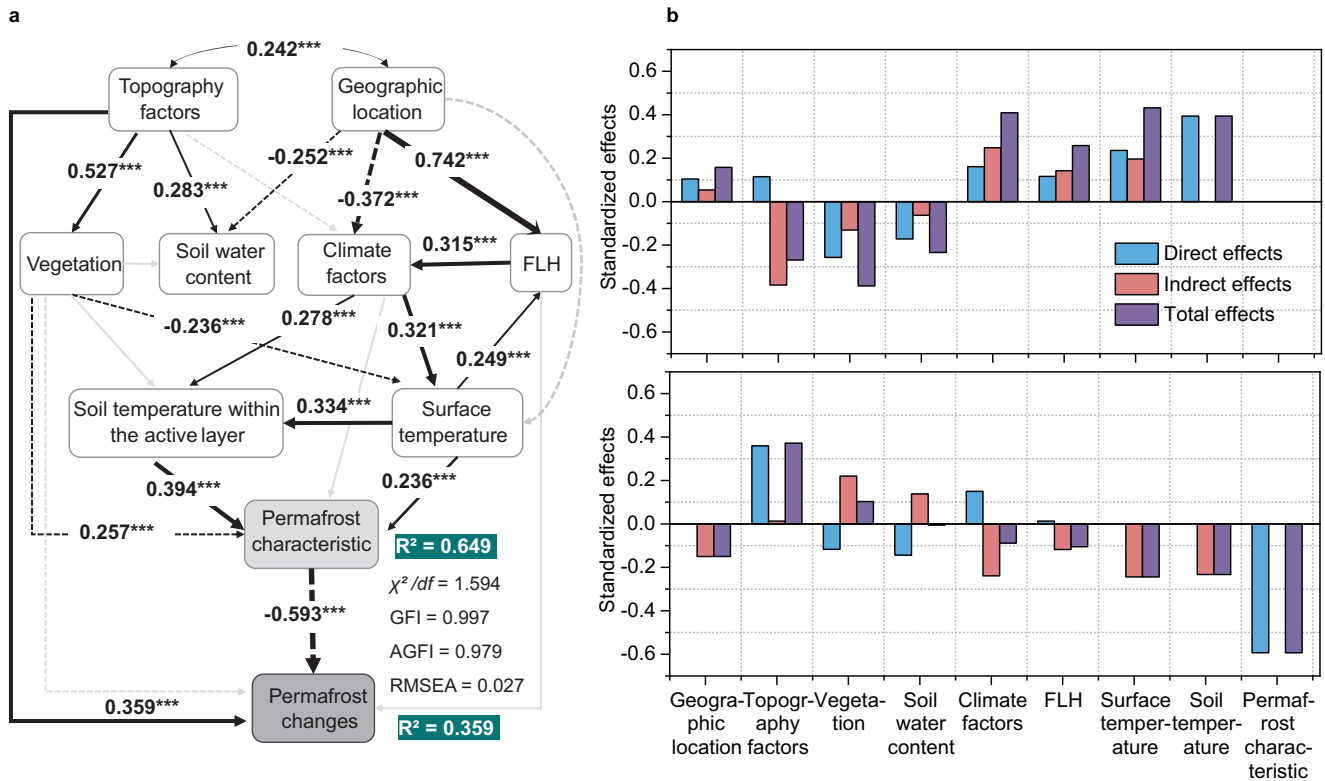**Fig. 5 | Structural equation model (SEM) analysis of environmental drivers affecting spatiotemporal changes in permafrost. a** Path diagram illustrating the hypothesized causal relationships. Single-headed arrows indicate the direction of causation. Black solid arrows indicate significant positive relationships, black dashed arrows indicate significant negative relationships, and gray arrows represent insignificant relationships. Rectangles represent the principal components for groups of climate variables: air temperature, precipitation, solar radiation, wind speed, surface pressure, and specific humidity; freezing level height (FLH); soil water content; and underlying factors including soil temperature and vegetation. Permafrost characteristics include active layer thickness (ALT), temperature at the top of permafrost (TTOP), and permafrost temperatures at 10 m and 15 m depths (PT_{10m}, PT_{15m}). Permafrost changes refer to changes in these attributes. Model fit indices reported are coefficient of determination (R^2), chi-square divided by degrees of freedom (χ^2/df), goodness of fit index (GFI), adjusted goodness of fit index (AGFI), and root mean square error of approximation (RMSEA). **b** bar graphs show the standardized direct, indirect, and total effects of environmental variables on permafrost characteristics (top panel) and permafrost changes (bottom panel). Asterisks indicate statistical significance (***$p < 0.001$).

Our study shows that vegetation impacts permafrost degradation both directly and indirectly, sometimes exerting opposite effects. Permafrost thawing increases, while permafrost warming decreases, as alpine meadows shift to alpine steppes and desert steppes. North of 34°N, accelerated permafrost degradation due to warming and wetting may lead to significant vegetation changes, including increased vegetation cover, biomass, nutrient levels, and root growth[18,42]. However, south of 34°N, warming and drying may cause the shrinkage of alpine wetlands, meadows, and steppes[18,43], potentially intensifying wind erosion[44] due to reduced water content and lowered supra-permafrost water level[43]. This vegetation change induced by permafrost degradation may threaten the sustainability of animal husbandry and the overall ecological integrity of the TP[16]. Additionally, accelerated permafrost degradation contributes to the rapid release of CO_2 and CH_4[45], especially during permafrost collapse[31,46].

The combined effects of engineering activities and climate change accelerate permafrost thawing, with the average thawing rate beneath embankment being 3 to 11 times larger than under natural surface, leading to strong subgrade settlement deformation[47]. A survey of embankment damage along the Qinghai-Tibet Highway shows that, despite renovations from 2008 to 2010, the damage rate remained over 30% by 2014[48]. In sections with high ice content, embankment damage exceeded 50%[49]. Due to permafrost thawing, 55 km of the Qinghai-Tibet Railway required extensive maintenance between 2010 to 2018[25,50]. Consequently, damage related to permafrost thaw has significantly increased operational costs for the Qinghai-Tibet Highway, amounting to ~US $680 million between 1986 and 2011[5,7].

The spatial variations in permafrost temperature and ALT changes across the TP remain poorly understood. Most of our permafrost observation sites are concentrated along the Qinghai-Tibet Railway, where permafrost borehole temperatures are continuously measured[51,52]. However, there are only a few observation sites in other regions, such as the eastern and western TP, where borehole temperatures are only measured a few times each year[53,54]. The data from those other sites have not been analyzed due to the relatively short time series (<10 years) compared to our primary data. Therefore, while we compile the most extensive in situ permafrost monitoring dataset of the TP, the availability of our field samples is still limited, restricting our ability to conduct more comprehensive statistical analyses on additional impacting factors. To address this gap, there is a need for more extensive monitoring data to better understand the uncertainties associated with permafrost degradation under climate change. With more data, we can also utilize state-of-the-art machine learning and artificial intelligence techniques to further enhance the accuracy of permafrost simulations and predictions, substantially improving our understanding and management of carbon and nitrogen emissions, water resources, ecological functions, and engineering service assessments in the permafrost regions of the TP.

Methods
Data collection
Permafrost characteristic: in characterizing permafrost attributes, we employ metrics including ALT, TTOP, PT_{10m} and PT_{15m}. The

observations of yearly mean data were sourced from the permafrost monitoring network (boreholes data) on the TP for the period 2001 to 2020. Notably, these data sequences exhibit disparate lengths[52,55,56], ranging from 1995-2020 to 2006-2020. To ensure data consistency across the study period, we extended shorter data sequences by incorporating information from nearby stations that exhibited strong correlations with the target site. Specifically, we applied a correlation threshold of $R^2 > 0.85$, a commonly accepted statistical criterion to ensure high consistency between the extended and original datasets. In cases where data were particularly limited and no suitable nearby stations were available, we compared the target site's data with all available data and adopted a stricter threshold of $R^2 > 0.95$ to further enhance the reliability of the extended data sequences. Sites with excessive missing data that could not meet these criteria were excluded from the analysis. We ended up compiling a dataset consisting of 77 unique boreholes. These boreholes cover a vast geographical range within the TP permafrost region, extending over 2000 kilometers from east to west and 550 kilometers from north to south (Supplementary Fig. 14). These retained boreholes exhibit varying elevations, ranging from 4200 to 5200 meters, and encompass mean annual ground temperatures ranging from higher than -0.5°C to lower than -3.0°C. Additionally, they cover various highland geomorphic types such as mountains, valleys, piedmont plains, and basins, as well as the major covering vegetation types, including alpine meadows (AM, characterized by dense vegetation cover), alpine steppes (AS, with sparser vegetation cover and more variable moisture conditions), and alpine desert steppes (ADS, characterized by very low vegetation cover, mostly consisting of drought-tolerant grasses). These vegetation types are dominant in the high-altitude regions of the TP and play critical roles in modulating permafrost dynamics. ALT, TTOP, PT_{10m} and PT_{15m} data primarily originate from 55 borehole monitoring sites in the central TP.

Environmental variables: we selected various environmental variables to investigate the impact of different environmental factors on the permafrost within the TP and its variations. These variables encompass geographic location factors (longitude, latitude, and elevation), terrain condition factors (slope, aspect, surface roughness (Rf)), and topographic degree of relief (DOR), land surface temperatures (LST), meteorological variables such as precipitation (Pre), 2-meter air temperatures (Ta), wind speed (Ws), Solar radiation (Sr), specific humidity (Sh), and near-surface atmospheric pressure (Sp). We considered vegetation coverage (VC) to describe vegetation conditions, soil ice content near the permafrost table as an indicator of permafrost ice state. Furthermore, we included the free-air freezing level heights (FLH) in summer over the TP as they represent the thermal state in the middle troposphere, reflecting a more stable indicator of climate change than air temperatures.

Soil ice content was uniformly converted to volumetric moisture content (VMC, vol. %). Slope, aspect, Rf, and DOR were calculated by ArcGIS software (V10.0), using Digital Elevation Model (DEM) data from the Japanese ALOS satellite with a resolution of 20 m (© JAXA/METI, accessed via the NASA Alaska Satellite Facility, https://asf.alaska.edu/data-sets), where the calculation neighborhood for DOR was determined as approximately 0.2 km² (20×20 pixels). Meteorological data were extracted by coordinates from the China meteorological forcing dataset provided by the China National Tibetan Plateau Data Center (TPDC) (https://doi.org/10.11888/AtmosphericPhysics.tpe.249369.file)[57]. This dataset was created by integrating existing international Princeton reanalysis data, GLDAS data, GEWEX-SRB radiation data, and TRMM precipitation data with conventional meteorological observation data from the China Meteorological Administration[57]. The dataset covers the period from 1979 to 2018 and provides annual average values with a horizontal spatial resolution of 0.1°×0.1°. Land surface temperature data is from the and surface temperature dataset for Western China (TRIMS LST-TP; 2000-2022) V2 of TPDC[58], which has a spatial resolution of 1 km. We used summer average FLH data (from

June to August) provided by Yi et al. (2022) based on ERA5 and NCEP/NCAR reanalysis data[59]. The FLHs data have a spatial resolution of 0.25°×0.25° and a temporal resolution of one year from 2001 to 2020.

Additionally, we consider the influence of engineering activities. The size of the engineering activity factor (EI) was determined using the Analytic Hierarchy Process. Considering the impact of engineering disturbances, four indicators were selected as the basis for evaluating the magnitude of the engineering factor: distance from the drilling location to the engineering site (H1), size of water puddles around the drilling site (H2), scope of vegetation removal around the borehole (H3), and distance from the borehole to the construction road (H4). The specific evaluation system and calculation methods are described in Supplementary Fig. 14.

Statistical Analysis

Permafrost change: Firstly, we conducted the Mann-Kendall trend test on the time series data for ALT, TTOP, PT_{10m}, and PT_{15m}. Liner trends, estimated by the least-squares method for sequences with statistically significant changes ($P < 0.05$), with the resulting slope representing the rate of change. We calculated the change rate of ALT (or permafrost temperatures) over a running time window (5-yr) from 2002 to 2020 and then obtained their trend of rate by liner regression. To robustly assess changes in permafrost, we calculated the frequency distribution of the average values of the time series data for ALT and permafrost temperatures during the initial 10 years and the final 10 years.

Attribution analysis: The statistical analyses were performed in the R software (V4.2.1; https://www.r-project.org/). The relative importance of different meteorological factors in permafrost changes over time was assessed using the Lindeman-Merenda-Gold method (LMG) which averages the sequential sums of squares over all orderings of repressors, which calculates the relative importance of each variable and ranks them (calculated by Relaimpo R package). To investigate the spatial variations of permafrost and it changes, we analyzed the relationship between various environment variables and permafrost characteristics, including ALT, TTOP, PT_{10m}, and PT_{15m} (mean values over the period 2001-2020), as well as their respective rates of change. We initially selected 18 environmental variables for analysis and generated a correlation coefficient matrix to evaluate their interrelationships (Supplementary Fig. 12). Variables that did not exhibit significant correlations with permafrost attributes were subsequently excluded (such as the engineering activity factor). Recognizing the presence of strong collinearity occurred among particular environmental factors, we employed cluster analysis (the varclus procedure in the Hmisc R package) to assess the collinearity or redundancy of environmental factors. Only one variable was selected for those clustered closely (30×Heoffding D > 0.6) as the representative variable (Supplementary Fig. 6). All variables were categorized into five groups: permafrost characteristics variables (ALT, TTOP, PT_{10m}, and PT_{15m}); permafrost change variables (changing rates of ALT, TTOP, PT_{10m}, and PT_{15m}); temperature factors (air temperature and land surface temperature); no-temperature environmental factors (meteorological variables except air temperature and other environmental factors such as latitude, altitude, slope, Rf, VC, and VMC). Variance partitioning analysis (VPA) based on canonical correlation analysis was utilized to understand the explanatory power of environmental factors. We then constructed a structural equation model (SEM) using AMOS 24.0.0 to elucidate the pathways through which each of these factors influences permafrost. Geography (latitude and altitude), topography (slope, Rf, and VC), climate (Pre, Ta, WS, Ra, Sh, and Sp), permafrost characteristic (ALT, TTOP, PT_{10m}, and PT_{15m}) and permafrost change (rates of ALT, TTOP, PT_{10m}, and PT_{15m}) variables were represented by their PC1 scores, which explained 86.26%, 55.96%, 49.76%, 76.39%, and 51.86% variance of corresponding environmental groups. The fit of the suitable model was judged by the χ2/df (<3), the GFI (>0.90), the AGFI (>0.90), and the RMSE (<0.05).

Data availability
Source data supporting the findings of this paper, including all active layer thickness (ALT) and permafrost temperature data, are publicly available in the Figshare data repository (https://doi.org/10.6084/m9.figshare.29206613.v1) as well as in the Supplementary Information. All data are freely accessible to readers without any application or approval required.

Code availability
No custom code or algorithm was developed for this study. All data analyses and figure generation were performed using standard statistical functions and procedures in SPSS (v26), OriginPro (v2023), only some analyses involved the use of R, where standard packages were directly applied as described in the Methods section. Therefore, no code files are necessary to reproduce the results.

References
1. Gruber, S. Derivation and analysis of a high-resolution estimate of global permafrost zonation. *Cryosphere* **6**, 221–233 (2012).
2. Schuur, E. A. G. Climate change and the permafrost carbon feedback. *Nature* **520**, 171–179 (2015).
3. Biskaborn, B. K. et al. Permafrost is warming at a global scale. *Nat. Commun.* **10**, 264 (2019).
4. Smith, S. L. et al. The changing thermal state of permafrost. *Nat. Rev. Earth Environ.* **3**, 10–23 (2022).
5. Hjort, J. et al. Impacts of permafrost degradation on infrastructure. *Nat. Rev. Earth. Environ.* **3**, 24–38 (2022).
6. Melvin A. M., et al. Climate change damages to Alaska public infrastructure and the economics of proactive adaptation. *Proc. Natl. Acad. Sci.* **114**, (2016). https://doi.org/10.1073/pnas.1611056113.
7. Ran, Y. et al. Permafrost degradation increases risk and large future costs of infrastructure on the Third Pole. *Commun. Earth Environ.* **3**, 238 (2022).
8. Miner, K. R. et al. Permafrost carbon emissions in a changing Arctic. *Nat. Rev. Earth Environ.* **3**, 55–67 (2022).
9. Hjort, J. et al. Degrading permafrost puts Arctic infrastructure at risk by mid-century. *Nat. Commun.* **9**, 5147 (2018).
10. Jin, H. et al. The infrastructure cost of permafrost degradation for the Northern Hemisphere. *Glob. Environ. Chang.* **84**, 102791 (2024).
11. Grosse, G. et al. Vulnerability and feedbacks of permafrost to climate change. *Eos Trans. AGU* **92**, 73 (2011).
12. Chadburn, S. et al. An observation-based constraint on permafrost loss as a function of global warming. *Nat. Clim. Chang.* **7**, 340–344 (2017).
13. Alessa, L. et al. Toward a Permafrost Vulnerability Index for critical infrastructure, community resilience and national security. *Geogr* **3**, 522–542 (2023).
14. Teufel, B. & Sushama, L. Abrupt changes across the Arctic permafrost region endanger northern development. *Nat. Clim. Chang* **9**, 858–862 (2019).
15. Ran, Y. et al. Distribution of permafrost in China – An overview of existing permafrost maps. *Permafr. Periglac. Process.* **23**, 322–333 (2012).
16. Cheng, G. et al. Characteristic, changes and impacts of permafrost on Qinghai-Tibet Plateau. *Chin. Sci. Bullet* **64**, 2783–2795 (2019). in Chinese.
17. Guo, D. & Wang, H. Simulated historical (1901–2010) changes in the permafrost extent and active layer thickness in the Northern Hemisphere. *J. Geophys. Res. Atmos.* **122**, 285–12 (2017).
18. Wang, G. et al. Climate changes and its impact on tundra ecosystem in Qinghai-Tibet Plateau, China. *Clim. Chang.* **106**, 463–482 (2011).
19. Wu, Q. et al. Engineering in the rugged permafrost terrain on the roof of the world under a warming climate. *Permafr. Periglac. Process* **31**, 417–428 (2020).
20. Ding, Y. et al. Adaptation research of cryosphere change. *J. Glaciol. Geocryol.* **42**, 11–22 (2020).
21. Li, Y. et al. Linkage between anomalies of pre-summer thawing of frozen soil over the Tibetan Plateau and summer precipitation in East Asia. *Environ. Res Lett.* **16**, 114030 (2021).
22. Yao, T. et al. The imbalance of the Asian water tower. *Nat. Rev. Earth Environ.* **3**, 619 (2022).
23. Zhao, L. et al. Changing climate and the permafrost environment on the Qinghai–Tibet (Xizang) Plateau. *Permafr. Periglac. Process* **31**, 396–405 (2020).
24. Zhang, Z. et al. Changes in the permafrost temperatures from 2003 to 2015 in the Qinghai-Tibet Plateau. *Cold Reg. Sci. Technol.* **169**, 102904 (2020).
25. Wu, Q. et al. Permafrost degradation threatening the Qinghai–Xizang railway. *Engr* **49**, 177–189 (2024).
26. Noetzli, J. et al. Enhanced warming of European mountain permafrost in the early 21st century. *Nat. Commun.* **15**, 10508 (2024).
27. Romanovsky, V. E. et al. H.H. Permafrost thermal state in the polar Northern Hemisphere during the international polar year 2007–2009: a synthesis. *Permafr. Periglac. Process* **21**, 106–116 (2010).
28. Xiao, Y. et al. Analyses of the influence factors of permafrost distribution on the Qinghai-Tibet Plateau based on geographical detector. *J. Glaciol. Geocryol.* **43**, 311–321 (2021).
29. Chen, D. et al. Assessment of past, present and future environmental changes on the Tibetan Plateau. *Chin. Sci. Bull.* **60**, 3025–3035 (2015).
30. Mu, C. et al. The status and stability of permafrost carbon on the Tibetan Plateau. *Earth Sci. Rev.* **211**, 103433 (2020).
31. Murton J. B. Permafrost and climate change. Clim Change pp. 281–326 (2021).
32. Romanovsky, V. E. et al. Past and recent changes in air and permafrost temperatures in eastern Siberia. *Glob. Planet. Chang.* **56**, 399–413 (2007).
33. Wang, K. et al. Permafrost thermal responses to asymmetrical climate changes: An integrated perspective. *Geophys. Res. Lett.* **50**, e2022GL100327 (2023).
34. Wang, X. et al. Contrasting characteristics, changes, and linkages of permafrost between the Arctic and the Third Pole. *Earth Sci. Rev.* **230**, 104042 (2022).
35. Grünberg, I. nge et al. Linking tundra vegetation, snow, soil temperature, and permafrost. *Biogeosciences* **17**, 4261–4279 (2020).
36. Che, T. et al. Snow cover variation and its impacts over the Qinghai-Tibet Plateau (In Chinese). *Bull. Chin. Acad. Sci.* **34**, 1247–1253 (2019).
37. Xu, W. et al. Spatial-temporal variability of snow cover and depth in the Qinghai-Tibetan Plateau. *J. Clim.* **30**, 1521–1533 (2017).
38. Hamm, A. et al. Continentality determines warming or cooling impact of heavy rainfall events on permafrost. *Nat. Commun.* **14**, 3578 (2023).
39. Magnússon, R. Í et al. Extremely wet summer events enhance permafrost thaw for multiple years in Siberian tundra. *Nat. Commun.* **13**, 1556 (2022).
40. Wang, Y. et al. Does the continuous wetting of the Tibetan Plateau contribute to the accelerated degradation of permafrost?. *Sci. China Earth Sci.* **67**, 1714–1718 (2024).
41. Miao, C. et al. Understanding the Asian water tower requires a redesigned precipitation observation strategy. *Proc. Natl. Acad. Sci.* **121**, e2403557121 (2024).
42. Jin, H. et al. Impacts of climate-induced permafrost degradation on vegetation: A review. *Adv. Clim. Chang. Res.* **12**, 29–47 (2021).
43. Yang, M. et al. Permafrost degradation and its environmental effects on the Tibetan Plateau: a review of recent research. *Earth Sci. Rev.* **103**, 31–44 (2010).
44. Dong, Z. et al. High-altitude Aeolian research on the Tibetan Plateau. *Rev. Geophys.* **55**, 864–901 (2017).

45. Chen, L. et al. Determinants of carbon release from the active layer and permafrost deposits on the Tibetan Plateau. *Nat. Commun.* **7**, 13046 (2016).

46. Wang, G. et al. Enhanced response of soil respiration to experimental warming upon thermokarst formation. *Nat. Geosci.* **17**, 532–538 (2024).

47. Jiang, G. et al. Long-term responses of permafrost to the dual impacts of climate warming and engineering disturbance along the Qinghai-Tibet Highway. *Cold Reg. Sci. Technol.* **220**, 104135 (2024).

48. Chai, M. et al. Characteristics of asphalt pavement damage in degradation permafrost regions: case study of the Qinghai–Tibet Highway, China. *J. Cold Reg. Eng.* **32**, 05018003 (2018).

49. Wu, Q., Zhang, Z. & Liu, G. Relationships between climate warming and engineering stability of permafrost on Qinghai-Tibet plateau. *J. Eng. Geol.* **29**, 342–352 (2021).

50. Zhang, S. et al. Evaluation of damage probability of railway embankments in permafrost regions in Qinghai–Tibet Plateau. *Eng. Geol.* **284**, 106027 (2021).

51. Wu, Q. & Zhang, T. Recent permafrost warming on the Qinghai-Tibetan Plateau. *J. Geophys. Res.* **113**, D13108 (2008).

52. Wu, Q. et al. thermal state of the active layer and permafrost along the Qinghai-Xizang (Tibet) Railway from 2006 to 2010. *Cryosphere* **6**, 607–612 (2012).

53. Luo, D. et al. Elevation-dependent thermal regime and dynamics of frozen ground in the Bayan Har Mountains, Qinghai-Tibet. *Plateau Permafr. Periglac. Process.* **29**, 257–270 (2018).

54. Zhao, L. et al. A synthesis dataset of permafrost thermal state for the Qinghai–Tibet (Xizang) Plateau, China. *Earth Syst. Sci. Data* **13**, 4207–4218 (2021).

55. Wu, Q. et al. Changes in active layer thickness and thermal state of permafrost between 2002 and 2012 in a variety of alpine ecosystems, Qinghai-Xizang (Tibet) Plateau, China. *Glob. Planet. Chang.* **124**, 149–155 (2015).

56. Zhang, Z. et al. Changes in permafrost temperatures from 2003 to 2015 on the Qinghai-Tibet Plateau. *Cold Reg. Sci. Technol.* **169**, 102904 (2019).

57. Zhao, L. et al. A synthesis dataset of permafrost thermal state for the Qinghai-Xizang (Tibet) Plateau, China. *Earth Syst. Sci. Data* **13**, 4207–4218 (2021).

58. He, J. et al. The first high-resolution meteorological forcing dataset for land process studies over China. *Sci. Data* **7**, 25 (2020).

59. Yi, Z. et al. Analysis of the 0°C level height variation over the Qinghai-Tibet Plateau in summer from 1979 to 2100. *J. Glaciol. Geocryol.* **44**, 34–45 (2022).

Author contributions

Z.F. and Q.W. are the first co-authors. Z.F. performed the statistical analysis, wrote the manuscript and created the figures. Q.W. designed the study and performed the field expeditions, and collaborated in analyzing data, writing, and revising the manuscript. A.C. collaborated in writing and revising the manuscript. L.W., S.G., G.J., A.Y., H.Y., and J.C. collected data and discussed the results. H.Y. performed the vegetation survey at the sites.

Competing interests

The authors declare no competing interests.

Additional information

Supplementary information The online version contains supplementary material available at https://doi.org/10.1038/s41467-025-63032-x.

Correspondence and requests for materials should be addressed to Qingbai Wu.

Peer review information *Nature Communications* thanks Donglin Guo, Ketil Isaksen, and the other anonymous reviewer(s) for their contribution to the peer review of this work. A peer review file is available.

Reprints and permissions information is available at http://www.nature.com/reprints

Publisher's note Springer Nature remains neutral with regard to jurisdictional claims in published maps and institutional affiliations.